MACHINE LEARNING-ACCELERATED CALIBRATION OF COMPLEX HEAT SOURCE MODELS FOR WELDING AND ADDITIVE MANUFACTURING PROCESS SIMULATION

Y. LUO*, A. KUDVA*, E. JANG**, S. MATAN*, N. M. VEGA MICHALAK*, J. A. PAULSON*, A. PERRAULT*, B. ALEXANDROV*

**The Ohio State University, Columbus, OH, USA*
***Electric Power Research Institute, Charlotte, NC, USA*

DOI 10.3217/978-3-99161-089-2-029, license CC BY 4.0

ABSTRACT

The heat source (HS) models dictate the spatial distribution of applied heat during welding and additive manufacturing processes, making it a critical factor for accurate simulation. However, the problem of calibrating the HS model, i.e., selecting parameters for it that match experimental conditions, has often been overlooked, with parameter selection relying on empirical heuristics and human trial-and-error. This lack of systematic calibration can lead to poor simulation performance and thus limits the expressiveness of HS models that can be used. We present a machine learning framework for efficiently calibrating HS parameters, thereby facilitating use of HS models with greater expressiveness and practical applicability than the conventional double-ellipsoidal Gaussian model. The effectiveness of the proposed methodology is validated through case studies involving spray transfer gas metal arc welding (GMAW) and pulsed GMAW additive manufacturing. Experimental validation, including comparisons of thermal histories and heat-affected zone properties, confirms strong alignment between simulation and real-world observations. This work provides a systematic framework for improving welding simulation accuracy by addressing the long-standing limitations of empirical HS models and facilitating the adoption of more expressive and precise modeling approaches. Ultimately, we conclude that (1) machine-learning optimization-based calibration of HS parameters significantly enhances simulation accuracy compared to using HS models that are calibrated using standard methods; (2) using our framework, expressive HS models that can represent complex energy distribution better align with experimental data compared to the standard double-ellipsoid Gaussian model.

Keywords: heat source modeling and calibration, finite element analysis, machine learning, Bayesian optimization

INTRODUCTION

Heat source (HS) models are a group of spatial density functions that describe the heat input distribution in the workpiece during welding and additive manufacturing (WAM) processes. They are widely used in simulation of high-temperature material joining processes in replacement of thermal and mechanical kinetic simulations which involve the complex interaction of heat transfer, phase transformation phenomena, non-linear material thermal properties and the fluid dynamics [1-6]. With the application of HS, the simulation of WAM processes can be simplified as a heat transfer problem, where the heat input is modeled as a moving HS that dissipates energy into the workpiece. Advances in high-performance computing have enabled large-scale simulations of WAM processes and optimization methods such as the Computational Design of Experiments (CDoE) [7,8]. Applying data-driven methods of simulation and optimization to complex multi-pass WAM processes involving complex structure poses two challenges to existing HS models: 1) complex structures may require highly customized HS distributions [9] that are difficult to manually calibrate; 2) long-horizon simulations that involve multiple weld passes and long welding duration may require multiple HS models, each of which is applied at a different stage of the process such that reacts to changes in heat distribution and mediates the simulation errors aggregated from simulations of previous weld passes. Compromising such errors is beyond the consideration of empirical calibration, and the human-constrained models are not expressive enough (capable to represent diverse thermal energy distributions) to represent the complex heat transfer and phase transformation phenomena.

Conventional methods that combine expressiveness-limited HS models with trial-and-error calibration following empirical heuristics have become a substantial bottleneck to the application of computational optimization methods to large scale simulations. After reviewing existing approaches to perform WAM processes simulations, we find that parameterized HS models are typically calibrated against experimental data, where the parameters are adjusted to minimize the difference between the simulation and the experimental results. The HS model parameters must be optimized to agree with experimental data because the heat input to the workpiece is not typically measurable experimentally. In practice, the double-ellipsoidal Gaussian (DEG) model [10] is the most frequently used HS model in WAM simulations. The DEG model typically outperforms simple heat sources (e.g., point heat sources [11], surface round heat source [12]), but the agreement it achieves is often imperfect (even when the parameters are set carefully, as we show in our experiments). However, despite this imperfection, higher dimensional HS models are not widely used. We speculate that this is primarily because of a combination of factors, including the perception that higher dimensional HS models require too much experimental data and computation to calibrate with standard approaches and the reduced human interpretability - it is more difficult to intuitively know how to set parameters, which is a barrier for standard approaches.

We hypothesize that the lack of successful high dimensional HS models has slowed down the application of computational methods in the WAM community, especially in complex and long-horizon tasks. In this paper, we propose a machine learning framework for efficiently calibrating HS parameters such that enable a new generation of HS models that are more expressive and practical. We validate the effectiveness of the proposed framework through case

studies involving spray transfer gas metal arc welding (GMAWs) and pulsed gas metal arc (GMAWp) additive manufacturing. The observed validation shows that the proposed calibrated heat source models reduced peak temperature prediction error and the predicted thermal histories well aligned with experiments for the GMAW and GMAW-p AM processes. Thus, we conclude that expressive HS models and efficient calibration methods can improve simulation accuracy.

RELATED WORK

In this section, we review related work in the analytical and numerical solution of welding dynamics (Section 0) to provide a background for welding process analysis and application of HS models. Additionally, we review parameter optimization methods for HS models (Section 0).

ANALYTICAL AND NUMERICAL SOLUTION OF HEAT TRANSFER ANALYSIS

Analytical and numerical approaches are two methods to perform heat transfer analysis. The analytical method requires mathematical modeling of the entire environment (i.e., material properties, boundary conditions, heat distribution, etc.) to derive the temperature field function by time and location, while numerical solution uses a discrete representation of the environment and state transition function (e.g., partial differentiate equation) to approach an error-bounded solution iteratively. In practice, the analytical method can only be applied in studies of simple structures, constant material properties, plain boundary conditions [9] and simple HS models [11,12]. Therefore, analytical solution is of limited use for the complex welding environments and processes [9,12-16].

Numerical methods can resolve environments involving complex structures, non-linear material properties, varying boundary conditions and non-plain processes. Transient simulation of welding processes became feasible with finite element model simulation, where de Freitas Teixeira et al. [17] points out that accurate modeling of the heat distribution is critical for resolving thermal dynamics in welding process. Ur Rehman et al. [18] adopts a Gaussian distribution model to compromise FEA-based analysis for WAM process. Eager and Tsai [19] quantifies the application of Gaussian HS models by implementing a simple distribution parameter with which aiming to fit the shape of heat distribution against the weld pool dimensions. Goldak et al. [10,20] adjusts the Gaussian-based HS model to account for the regional contraction and expansion effects of heat distribution caused by moving HSs, introducing the double-ellipsoidal Gaussian (DEG) model. Its extensions later become prevalent in subsequent studies [21-26]. However, the DEG model is prone to over-simplifying the heat distribution especially for a weld pool with deep penetration [10], and in the central region of the weld pool where the simulation results are sensitive to the HS model [16,27]. For such cases, Wahab et al. [16] uses a composite HS model to represent both the surface arc energy and the droplet energy in gas metal arc welding, however the selected spherical heat source model is

not able to represent finger-like penetrations that are common to see in high heat input GMAW processes.

PARAMETER OPTIMIZATION FOR HEAT SOURCE MODELS

Goldak et al. proposed the DEG model along with an empirical parameterization method that is based on the weld pool dimensions [10,20]. Based on the DEG model, following studies have been conducted to characterize the HS model parameters [17,28,29] by evaluating how the simulated heat-affected zone (HAZ) or the thermal history align with the experimental results. Other studies model the fluid flow in the weld pool [1,4,11,30] and show this modeling leads to better determination of HS parameters. Optimization-based approaches have also been explored. SysWeld™ provides a Heat Source Fitting module that optimizes the HS model parameters by allowing users to iteratively adjust the parameters, thus approaches the experimental morphology of the weld pool [31,32]. Luo [7] developed a brute-force grid search method to calibrate heat source parameters for gas tungsten arc welding (GTAW) process simulation, which formally defines the calibration problem as a parameter optimization problem, but has low computational efficiency. Although there have been studies in parameterization of HS models, to our best knowledge, there is no discussion in developing HS models for matching weld pools resulting from different fluid patterns, nor in the application of machine learning methods to calibrate HS model parameters.

PRELIMINARIES

In this section, we review the double-ellipsoidal Gaussian HS model and cylinder-semi-sphere HS model, then provide background on the optimization methods that are related to this work.

HEAT SOURCE MODELS

Double Ellipsoidal Gaussian Model (DEG) [10] is the most widely used HS model in WAM practice. The DEG model uses two ellipsoids to model the heat distribution for the pre- and post-weld region respectively. We rewrite the HS model to depend on the parameters $(\sigma_x, \sigma_y, \sigma_z, \alpha_x^+, \dots, \alpha_z^-, k)$, with $\sigma_{h\in\{x,y,z\}} > 0$ as the boundary at the corresponding axis. Let Q (J/mm) be the heat input rate, and $q(0)$ be the maximum flux at the center of DEG model, defined by:

$$q(0) = \frac{2k^{1.5}Q}{\sigma_x\sigma_y\sigma_z\pi^{1.5}}$$

As the $+y$ is the welding direction, σ_x, σ_y and σ_z represent the width, length and depth of the heat source respectively. α_y^+ and α_y^- are the correction factors at the $+y$ and $-y$ octants that model the pre-weld contraction ($\alpha_y^+ < 1$) and post-weld extension ($\alpha_y^- > 1$) effects.

Similarly, $\alpha_x^+, \alpha_x^-, \alpha_z^+, \alpha_z^-$ allow adjusting boundaries at the HS width and depth, even though they are mostly kept 1 to ensure symmetric width and depth in practice. While the aforementioned parameters control the geometric representation of the DEG model, k controls the spreading of the energy distribution – DEG models with large k have more energy near HS center and vise verse.

$$\forall h \in \{x, y, z\}, \alpha_h = \begin{cases} \alpha_h^+, h \geq 0 \\ \alpha_h^- \text{ otherwise} \end{cases} \quad (1)$$

With the help of the indicator function (Equation (1)), the flux distribution of DEG model is defined as Equation (2).

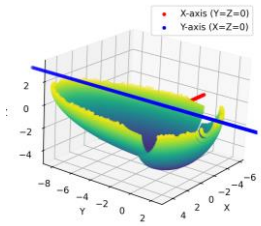

$$q_{DEG}(x, y, z) = q(0) \exp\left(\sum_{h \in \{x,y,z\}} -\frac{k\alpha_h^2 h^2}{\sigma_h^2}\right) \quad (2)$$

Fig. 1 Boundary of the DEG model

Fig. 1 shows the surface boundary of DEG model at which the energy intensity $q_{DEG} = fq(0)$. Goldak et al. [10] defined the default value of the parameters as $f = 0.05$, while $\sigma_x, \sigma_z, \sigma_y$ are directly taken from the weld pool width, depth, and length. We used the DEG model parameterized by this method as the baseline HS model and refer to it as empirical DEG model for the rest of paper.

Cylinder-Semi-Sphere (CSP) model uses a cylinder with a semi-sphere attached, to model the heat distribution with deep penetration. This model is implemented in SysWeld™ for users to use. It is parameterized by (r_t, r_b, h_t, h_b, k), where r_t, r_b are the top and bottom radiuses of the cylinder, and h_t, h_b are the top and bottom height of the cylinder. A semi-sphere is attached to the bottom of the cylinder with radius r_b. The cylinder-semi-Sphere model is defined as Equation (3).

$$R(x, y, z) = \begin{cases} r_t * \dfrac{z - h_b}{h_t - h_b} + r_b * \dfrac{h_t - z}{h_t - h_b}, h_b \leq z \leq h_t \\ r_b, h_b - r_b \leq z < h_b \\ 0, \quad \text{otherwise} \end{cases}$$

$$r(x, y, z) = \begin{cases} \left|\left|(0,0,z), (x,y,z)\right|\right|^2, h_b \leq z \leq h_t \\ \left|\left|(0,0,h_b), (x,y,z)\right|\right|^2, h_b - r_b \leq z < h_b \\ \infty, \quad \text{otherwise} \end{cases} \quad (3)$$

$$q_{CSP}(x, y, z) = q(0) \exp\left(-k \frac{r(x, y, z)}{R(x, y, z)}\right)$$

Where for each point (x, y, z) in the space, $R(x, y, z)$ represents the distance from its closest point p on the HS axis to where the ray line $(p, (x, y, z))$ falls on the boundary; and $r(x, y, z)$ are the distance from (x, y, z) to the p. Like the DEG model, k controls the spreading of the HS energy for the CSP model.

FLUID FLOW AND HEAT DISTRIBUTION

In arc welding, the distribution of the temperature field is affected by the convective fluid flow, the electromagnetic field, and the surface tension [3-6,16]. Such complex interaction has resulted in different fluid flow patterns in the weld pool. Mills et al. and Li et al. [3, 33] identify three major different weld pool flow patterns caused by the material surface-tension-temperature gradient ($\frac{d\gamma}{dT}$) in liquid phase. Inward flow is observed when $\frac{d\gamma}{dT} > 0$, where the surface flow gets pulled inward, such that the center flow flushes the substrate, causing penetration that is significantly deeper than usual weld pool (Fig. 2a). When under negative $\frac{d\gamma}{dT}$, the surface flow is pushed outward thus spreads to the side of the weld pool, causing the weld pool to have a flat bottom as shown in Fig. 2b. In the case of non-monotonicity of $\frac{d\gamma}{dT}$, the liquid in between the side and center reaches a peak surface-tension, pulling flow from both weld pool center and sides, indicated by Fig. 2c.

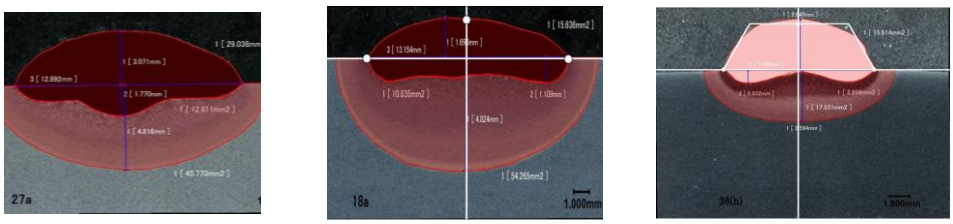

(a) $\frac{d\gamma}{dT} > 0$ (b) $\frac{d\gamma}{dT} < 0$ (c) Non-monotonic γ

Fig. 2 Cross-sections of typical weld pools in GTAW

To take these fluid flow patterns into account, HS models that can model more complex distribution (i.e., more expressive) than DEG and CSP models are needed. Previous HS models [10-12,20] are designed in ideal conditions where phenomena beyond the torch and arc energy distribution, such as fluid flow patterns, are not considered.

PARAMETER OPTIMIZATION METHODS

Parameter optimization aims at searching for optimal parameters against an objective function. For scenarios with expensive evaluations and black-box settings, Bayesian optimization is one popular method. Recently, first-order gradient descent methods have drawn significant attention due to their successes in deep neural network optimization.

Bayesian Optimization

Bayesian optimization (BO) is a sample-efficient method for optimizing costly, black-box functions. BO uses a probabilistic surrogate model, typically a Gaussian process (GP) [34], to model the unknown objective function and guide sampling through an acquisition function.

Let the HS model be represented as a function $f(h)$, where $h \in \mathcal{H} \subset R^d$ denotes a vector of model parameters in the HS parameter space $\mathcal{H}$. The goal is to solve the calibration problem:

$$h^* = argmin_{h\in\mathcal{H}}\, \mathcal{L}(f(h), y_{exp})$$

where $\mathcal{L}$ is a loss function (e.g., mean squared error) comparing model predictions $f(h)$ to experimental measurements y_{exp}. Since direct evaluation of $f(h)$ involves computationally intensive simulations, BO constructs a surrogate $\bar{f}(h) \sim GP(\mu(h),\ k(h,h'))$, where μ and k denote the predictive mean and covariance.

An acquisition function $\Psi(h;\ D)$, defined based on the GP posterior over $\mathcal{H}$, is then maximized to select the next evaluation point:

$$h_{t+1} = argmax_{h\in\mathcal{H}}\Psi(h; D_t)$$

where $D_t = \{(h_i, L_i)\}_{i=1}^{t}$ is the set of evaluated points and observed losses up to iteration t . After each new evaluation, the surrogate model is updated, and the process is repeated until a stopping criterion is met.

Gradient-based Optimization

The most important application of gradient-based optimization is in training deep neural networks (DNN) that potentially approximate arbitrary distributions [35, 36]. In training neural networks, the parameters (θ) of neural networks are optimized for minimal prediction loss with a set of sample and gold values (X, Y), where $X = [x_0, \dots, x_{|X|}], Y = [y_0, \dots, y_{|X|}]$:

$$\theta = argmin_{\theta\in\mathcal{R}^d}\left|\left|DNN_\theta(X), Y\right|\right|^2$$

Let $\mathcal{L}(X) = \left|\left|DNN_\theta(X), Y\right|\right|^2$, assuming that the true mapping $f^\star: X^\star \to Y^\star$ is a smooth function, then the gradient $\frac{\partial\mathcal{L}(X)}{\partial\theta}$ is applied to minimize the prediction loss ($\mathcal{L}$):

$$\theta = \theta - lr * \frac{\partial \mathcal{L}(X)}{\partial \theta}$$

where *lr* is the learning rate.

HEAT SOURCE CALIBRATION

We propose to **precisely** match the post-weld fusion boundary line (FBL) in HS calibration to account for the complex multifactor phenomena in the weld pool - instead of modeling the complex interactions, a surrogate is adopted by matching their combined effect to the HAZ that can be observed from the post-weld cross-sections. This is accomplished by adopting a more expressive HS models (Section 0) that can represent the complex heat distribution in the weld pool combined with machine learning-based optimization methods to calibrate the HS model parameters for matching the post-weld FBL (Section 0 and 0).

NEW HEAT SOURCE MODELS

In this section, two new HS models are proposed to address the limitation of the existing DEG model. The first model, called Double-ellipsoidal Gaussian and Cylinder-semi-Sphere (DEGC) model (Fig. 3a), is composed of a DEG model and a CSP model, alike to the approach as Champagne and Pham [37]. The DEGC model is designed to represent the phenomena observed in Fig. 2a. The second model, Dual Double-ellipsoidal Gaussian (DDEG) HS model (Fig. 3b), combines two identical DEG models, but with different energy intensities, such that it represents the complex flow phenomena observed in Fig. 2c, where negative $\frac{d\gamma}{dT}$ cases as Fig. 2b can be represented by the DEG model.

Double-Ellipsoidal Gaussian and Cylinder-semi-Sphere Model (DEGC) The weld pool with deep penetration is hard to model with DEG model, as it neglects the heat flow in the z direction [10]. To address the challenge of modeling deep penetration, the DEGC model couples a DEG model on top of a CSP model. Based on Equation (2) and (3), we can define the DEGC model as Equation (4), and the HS boundary is shown in Fig. 3a.

$$q_{DEGC}(x,y,z) = h_r q_{CSP}(x,y,z) + (1-h_r) q_{DEG}(x,y,z) \tag{4}$$

(a) DEGC **(b) DDEG**

Fig. 3 HS boundaries of the DDEG and DEGC heat source model

Where h_r adjust the energy split to the CSP and DEG HSs. Note that both the DEG and CSP are special cases of DEGC, corresponding to $h_r = 0$ and $h_r = 1$, respectively.

Dual Double-Ellipsoidal Gaussian Model (DDEG) is modified from the DEG model by composing two identical DEG models, where the energy intensity levels of the two models are adjusted by the indicator r_x ($r_x^+ + r_x^- = 2$) and the distance between the two models d. The HS model is defined as Equation (5), whose HS boundary is shown in Fig. 3b.

$$q_{DDEG}(x,y,z) = r_x q(0) \exp\left(-\frac{k\alpha_x^2(|x|-d)^2}{\sigma_x} - \frac{k\alpha_y^2 y^2}{\sigma_y^2} - \frac{k\alpha_z^2 z^2}{\sigma_z^2}\right) \quad (5)$$

The DDEG model is designed to capture the complex flow phenomena as shown in Fig. 2c: the liquid flow creates a "W" shape fusion line in the weld pool, which when simulating the heat distribution with DEG model, would need modeling two heat centers. Note that the DEG model is a special case of DDEG model (i.e., when $r_x = 1, d = 0$).

HEAT SOURCE CALIBRATION

The HS models introduced in Section 0 come with the cost of increasing the number of parameters that must be fit. To address the challenge of calibrating the HS model parameters in the context of the experimental weld HAZ properties, we introduce a heat source calibration framework that can optimize HS model parameters more efficiently.

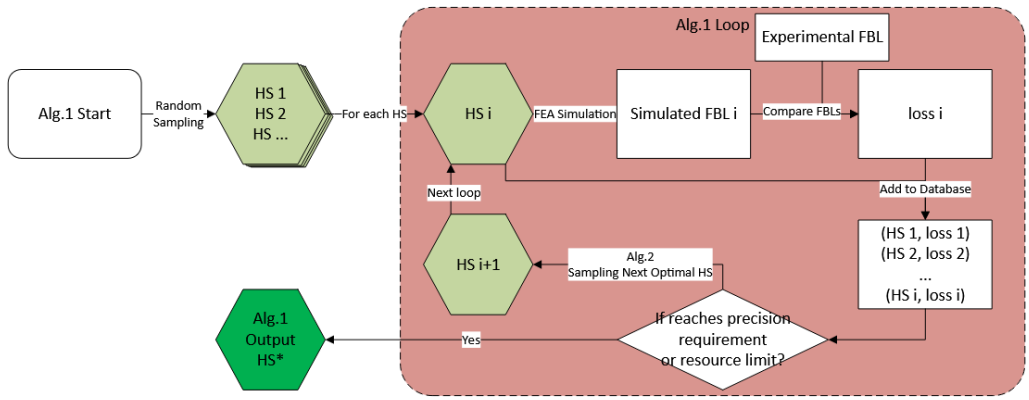

Fig. 4 Heat Source Calibration Framework

Alg. 1 Heat Source Calibration (HSC)

Input:

FEA: Finite Element Model
$\mathcal{H}$: Heat Source Parameter Space
τ_ω: The HAZ properties of goal experimental weld
φ_ω: The Welding parameters of goal experimental weld
$loss(\tau_\delta, \tau_\omega)$: The heat source evaluation function.
$\bar{\mathcal{S}}$: Upper limit of the calibration cases

1: $fl_\omega \sim \tau_\omega$ # Extract fusion line from HAZ of τ_ω
2: $\mathcal{S} = \emptyset$ # Initialized the set of explored HSs
3: $while\ |\mathcal{S}| < \bar{\mathcal{S}}\ do$
4: $h \sim \mathcal{H}/\mathcal{S}$ # Sample a HS parameter h with **Alg. 2**
5: $\tau_\delta^h = FEA(h, \varphi_\omega)$ # Run weld simulation with h and φ_ω
6: $l_h = loss(\tau_\delta^h, \tau_\omega)$ # Calculate the loss value for h
7: $\mathcal{S} = \mathcal{S} \cup \{(h, l_h)\}$ # Add h and its loss value l_h to $\mathcal{S}$
8: $end\ while$ # Reach calibration limit
9: return $h_\omega = argmin_{(h,l_h)\in\mathcal{S}} l_h$

Rather than intuitively selecting the parameters according to the experimental weld followed by the trial-and-error method, we introduce a machine learning framework to calibrate the HS model parameters**.** Alg. 1 and Fig. 4 shows the HS calibration procedure which aims to optimize the HS model by repeatedly sampling the potentially better HS model, calculating its loss in simulation, and, when the simulation budget is reached, returning the HS model parameters with lowest loss. Formally, the calibration goal is to match the FBL (τ_ω) that have been extracted from the experimental weld piece by setting the parameters of the HS model (h_ω) to minimize the simulation error (Δ) when it is used in a simulation along with the welding parameters φ_ω from the experimental weld:

$$h_\omega = argmin_{h\in\mathcal{H}} \Delta(\tau_h^\varphi, \tau_\omega^\varphi)$$

In this paper, we use fusion boundary line (FBL) as the calibration target, because FBL can be observed for many dissimilar metal welding processes using simple image processing methods. For other processes where FBL is indistinguishable, hardness value could be used as calibration criteria if there comes accurate predictive method that relates thermal history to hardness value [38,39]. Contrasting to the Heat Source Fitting module in SysWeld™ that relies on manual interactive adjustment of HS parameters, the principle of the HSC framework is adopting data-driven approach to benefits from all parameters been explored. The data-driven method ensures that all explored HS parameters contribute to profile the HS parameter space, with which, intelligent sampling method can approach global optimal HS efficiently and with confidence. The sampling method omitted Line 4 is introduced in Alg. 2**.**

MACHINE LEARNING-ACCELERATED CALIBRATION

The sampling of the new HS model parameters (h) (Line 4) in the parameter space $\mathcal{H}$ is a crucial step in the HS calibration process. For efficient calibration, the sampling strategy should balance exploration and exploitation in the parameter space, where exploration refers

to searching for new regions in the parameter space that may yield better results, and exploitation refers to refining the search around known good regions.

To achieve this balance, we propose a two-stage hybrid optimization strategy (Alg. 2) for the heat source calibration. Given the set of explored heat source and loss pairs $\mathcal{S}$, we first fit the surrogate model $Q_\theta(h)$ to predict the loss value associated with each heat source parameter h **(**Line 1-3). $Q_\theta(h)$ is a deep neural network (DNN) that takes the heat source model parameters h as input and outputs the loss value. θ is the parameters of the DNN to be trained on the data s. Then in the first sampling stage (Line 4), we use Bayesian optimization (BO) combined with upper confidence bound acquisition function [40] to explore the parameter space and identify potentially optimal regions (near h in Line 5). In the second stage (Line 5-7), we apply a gradient-based optimization method to locally fine-tune the parameter values from the best-found candidate. This hybrid approach enables reliable and sample-efficient calibration based on experimental fusion zone data.

Alg. 2 Hybrid Learning-Accelerated Calibration (HLAC)

Input:

$\mathcal{S} = \{(h, l_h), \dots\}$
$Q_\theta(h) = f: \mathcal{H} \to R$
l : Learning Rate
K: Learning Steps
k: Sampling Steps

1: $for\ i = 1 \to K\ do$
2: $\quad \theta = \theta - E_{h\in\mathcal{S}}\left[l\frac{\partial[MSE(Q_\theta(h),l_h)}{\partial\theta}\right]$ # Update the surrogate model
3: $end\ for$
4: $f(h) \sim\ GP(\mu_{(h,l)\in\mathcal{S}}(h), k_{(h,l),(h',l')\in\mathcal{S}}(h,h'))$ # Learn Gaussian process function $f(h)$
5: $h = argmax_{h\in\mathcal{H}}\ \Psi(h;\mathcal{S})$
6: $for\ i = 1 \to k\ do$
7: $\quad h' = h' - l\ \frac{\partial[Q_\theta(h')]}{\partial h'}$
8: $end\ for$
9: return h' # Return the new HS parameter

EVALUATION

The proposed DEGC and DDEG HS models (Section 0) and the machine learning-accelerated calibration method (Section 0) are demonstrated and evaluated in this section. The evaluation is conducted by physical experiments and FEA simulations of spray arc gas metal arc welding (GMAWs) and pulsed arc gas metal welding (GMAWp) wire-arc direct energy deposition (WA-DED) processes. For each process, we run HS calibration (Alg. 1) with the proposed HS models in Section 0 and the HLAC method (Alg. 2).

EXPERIMENTAL SETUP AND MODELING SETUPS

GMAWs bead on plate weld HHI, MHI, and LHI welds is used in HS calibration for FEA modeling of multi-pass groove welds in Fe-10Ni steel [41]. The GMAWP WA-DED process

is developed for a single bead per layer additive build of a high strength steel (HSS) [42]. Table 1 **s**hows the welding parameters used with the three processes.

Table 1 Experimental Setup for the GMAWs and GMAWp processes

	GMAWs			GMAWp – WA-DED
	LHI	**MHI**	**HHI**	
Base Material	Fe-10Ni			A36 steel
Filler Material	Fe-10Ni			HSS
Voltage V	27			17.3
Current A	300			174
Heat Input J/mm	993	1574	2204	819
Travel Speed mm/s	7.9	5.04	3.8	4.23-5.93
Wire Feed Rate mm/s	139			245
Wire Diameter mm	1.14			1.14

The thermal histories experienced in the heat affected zones (HAZ) of these welds and builds are recorded using 0.2 mm diameter Type C thermocouples and a fast-sampling data acquisition system. The thermocouples are installed in ceramic insulators and capacitor-discharge welded to the tips of 1.8 mm diameter holes, located within 1 to 4 mm distance from the anticipated fusion boundaries, as shown in Fig. 5a. The welds and the WA-DED build are cross sectioned, prepared for characterization using standard metallography techniques, and the FBLs extracted using the image processing software ImageJ™.

FEA models of the two processes are developed in SysWeld™ using fusion zone and HAZ mesh size of 0.5 mm. The FEA models are run with process parameters and material properties of the respective base and weld filler metals listed in Table 1. Cross sections of a GMAWs bead on plate weld, and a GMAWp WA-DED build, their respective FEA models used in the HS calibration and evaluation procedures, and extracted FBLs are respectively shown in Fig. 5 and Fig. 6**.**

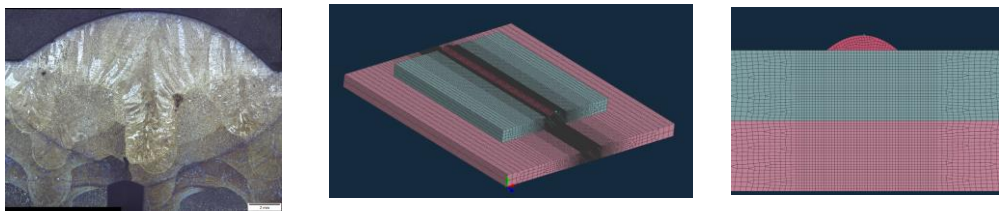

(a) (b)

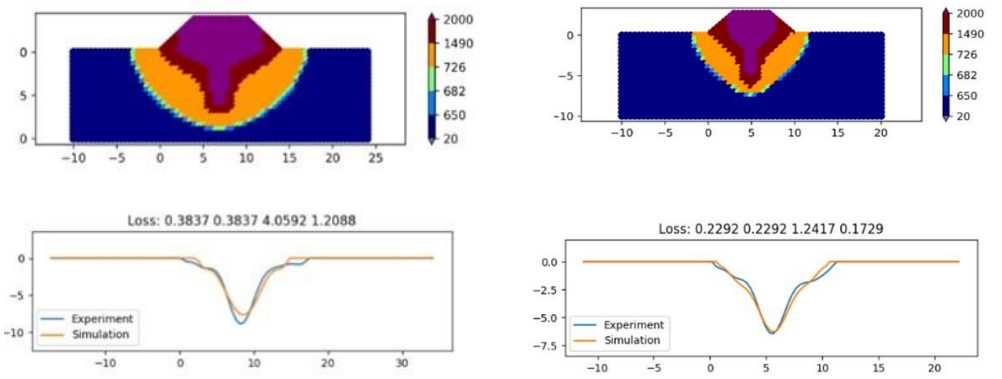

(c) (d)

Fig. 5 GMAWs bead on plate weld: a) HHI bead cross section with thermocouple hole location, b) FEA model: weld bead deposited over Fe-10Ni overlay on low alloy steel substrate; experimentally extracted and DEGC HS calibrated FBLs: c) HHI, d) LHI

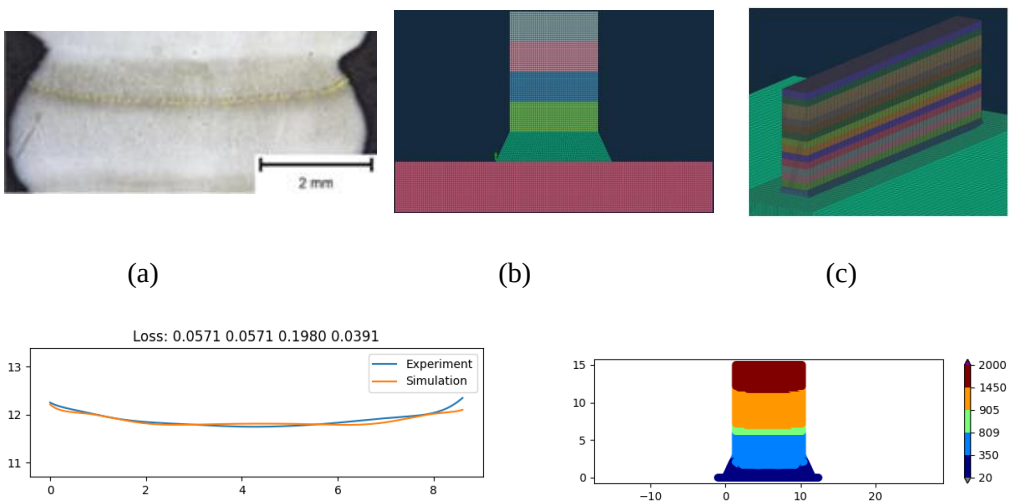

(a) (b) (c)

(d)

Fig. 6 GMAWp WA-DED build: a) build cross section with highlighted FBL, b) FEA model, c) experimentally extracted and DDEG HS calibrated FB

HEAT SOURCE CALIBRATION

For the calibration criteria, we use the FBLs extracted from the experimental welds as the target FBLs. The loss function is defined as the mean square error (MSE) between the simulation and the experimental FBLs as Equation (6).

$$loss_{fl}(\tau_h^{\varphi}, \tau_{\omega}^{\varphi}) = \int_{x_0}^{x_1} \left\| fl_h^{\varphi(x)} - fl_{\omega}^{\varphi}(x) \right\|^2 dx \tag{6}$$

where $fl_h^{\varphi}(x)$ is the FBL of the simulation with HS model h, and $fl_{\omega}^{\varphi}(x)$ is the FBL of the experimental weld, both with welding parameters γ (Table 1). The parameters of the calibrated GMAWS and GMAWP WA-DED heat sources are listed in Table 2.

Table 2 Calibrated HS models and parameters

Heat Source	**GMAWs** [41]			**GMAWp – AM** [42]
	LHI	**MHI**	**HHI**	
Name		DEGC		DDEG
$\sigma_x, \sigma_y, \sigma_z\ (mm)$	10,6,1	16,8,3	6,3,0.5	11.67,6.17,0.16
k		1		0.53
α_y^+, α_y^-		1		1
α_x, α_z		1		1
$d\ (mm)$		0		1.21
$r_t, r_b\ (mm)$	2,3	3,4	2,3	-
$h_t, h_b\ (mm)$	1.5, -1.5	2.5, -2.5	1.5, -1.5	-
$h_{r(mm)}$	0.27	0.27	0.36	-

Images of FEA predicted FLBs using the respective DDEG and DEGC heat source models are shown in Fig. 5c, Fig. 5d and Fig. 6d . There is a very good correlation between the FEA predicted and experimentally extracted FBLs. This demonstrates the capability of the developed DDEG and DEGC heat source models and of the calibration procedure to accurately simulate the fusion boundary regions generated by GMAWs and GMAWp WA-DED processes.

VALIDATION

The validation of the calibrated HS model compares the simulation and the experimental thermal histories and HAZ properties. Particularly, we run extensive simulation of the experimental welds, then compare the simulation thermal history with the experimental thermal history and compare the predicted with the experimental HAZ properties (hardness and microstructure). We additionally run simulation of the GMAPp WA-DED processes with DEG model, parameterized according to the empirical method in Goldak et al. [10].

As demonstrated in Fig. 7, Table 3 and Table 4, the predicted thermal histories using calibrated DEGC and DDEG heat sources closely match the measured ones in terms of peak temperatures, heating and cooling rates.

The average error of the predicted peak temperature for the calibrated DDEG heat source model is between 0.3% and 3.4% while that for the calibrated DEGC model is between 0.8% and 4.1%. The small errors in predicting the thermal cycles parameters demonstrate the accuracy of the developed DDEG and DEGC heat source models and the HS calibration procedure.

The temperature range of multiple reheat tempering in steels is located between the AC3 temperature and a minimum tempering temperature (MTT) [43], Fig. 7b. Accurate prediction of multiple reheat thermal histories in that temperature range is of importance for efficient process optimization in temper bead welding and additive manufacturing. As shown in Fig. 7b and Table 3, the DDEG heat source demonstrated better accuracy in predicting peak temperatures and cooling times in that temperature range compared to the classical DEG heat source model.

Table 3 Peak temperature and cooling rate comparison for GMAW-p process simulated with calibrated DDEG HS

	Peak Temperature [C]					
Heat Source	**DDEG**			**DEG**		
Thermal Cycle #	**Predicted**	**Measured**	**Error (%)**	**Predicted**	**Measured**	**Error (%)**
1	681	686	0.7	725	686	5.4
2	572	565	1.2	592	565	4.6
3	496	491	1.0	506	491	3.0
4	441	435	1.4	435	435	0
5	397	398	0.3	393	398	1.3
6	363	372	3.4	357	372	4.0
	Cooling Time $\Delta t_p/MTT$ (s)					
Heat Source	**DDEG**			**DEG**		
Thermal Cycle #	**Predicted**	**Measured**	**Error (%)**	**Predicted**	**Measured**	**Error (%)**
1	13.22	13.60	2.8	14.17	13.70	3.3
2	8.86	8.57	3.4	9.39	8.57	8.7
3	6.33	6.11	3.6	6.37	6.11	4.1
4	4	3.93	1.8	4.25	3.93	7.5
5	2.77	2.47	12.1	2.90	2.47	14.8

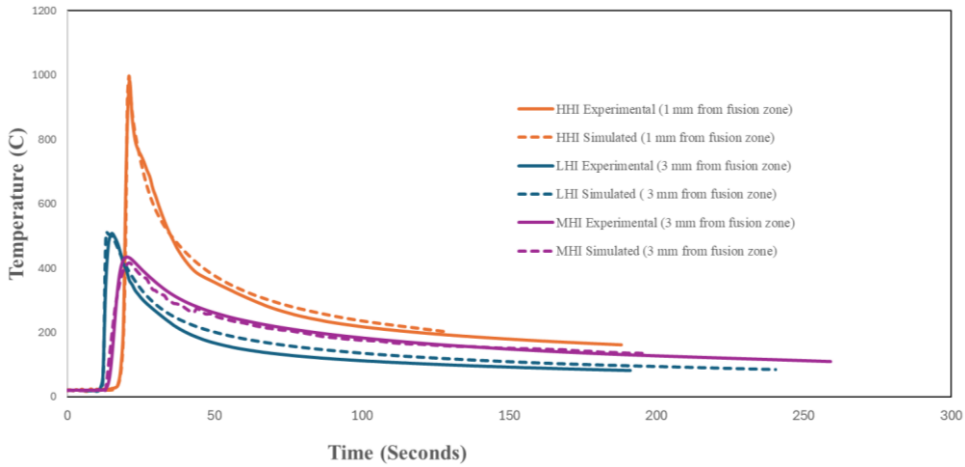

(a) GMAW with DEGC model

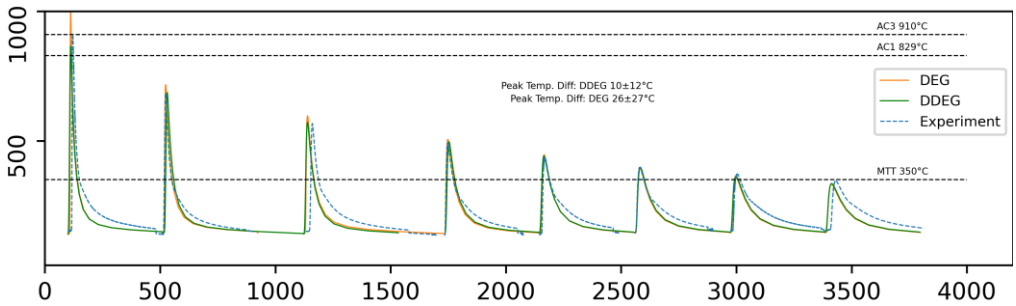

(b) GMAWp-AM

Fig. 7 Thermal history validation for GMAW and GMAW-AM processes

Table 4 Peak temperature and cooling time comparison for GMAWs process simulated with calibrated DEGC HS

Heat Input	Peak Temperature [C]			$\Delta t_p/MTT\ (s)$		
kJ/mm	Predicted	Measured	Error (%)	Predicted	Measured	Error (%)
LHI 25	511	507	0.8	17	20	15
MHI 40	433	416	4.1	7.5	8.5	11.7
HHI 55	998	979	1.9	32.2	34	6

The developed DDEG and DEGC heat source models and the heat source calibration method are extensively used for microstructure and property predictions, and process optimization in welding and additive manufacturing. Examples of such applications for predicting

hardness distribution in multi-pass GMAWs build in Fe-10Ni steel [41]and in a single pas per layer GMAWp WA-DED build in HSS [42] are shown in Fig. 8 and Fig. 9, respectively.

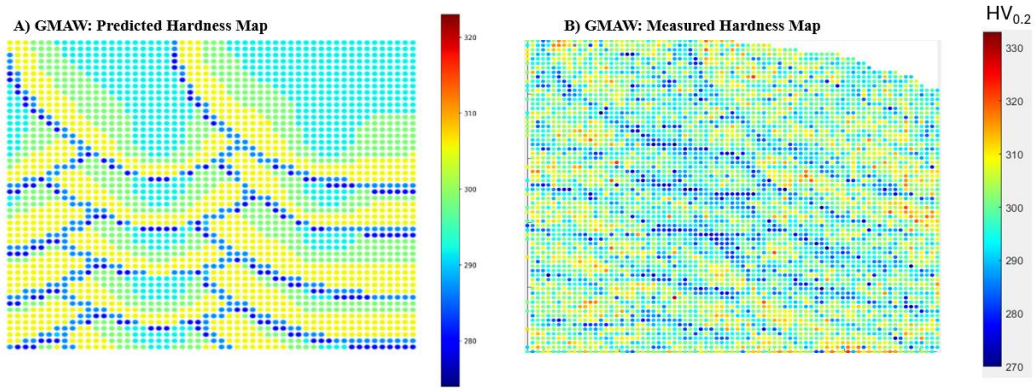

Fig. 8 Example application of calibrated DEGC heat source in FEA hardness prediction in a GMAWs muti-pass build in Fe-10Ni steel: a) predicted hardness map, b) experimentally generated hardness map

The predicted hardness map in Fig. 8a was developed by FEA modeling of a GMAWs processes using the MHI processes parameters in Table 1, the DGEC heat source in Table 2, and experimentally developed thermal history - hardness relationships [41]. The hardness map in Fig. 8b was generated using LECO LM 100AT hardness mapper with 200g load and 350 μm step.

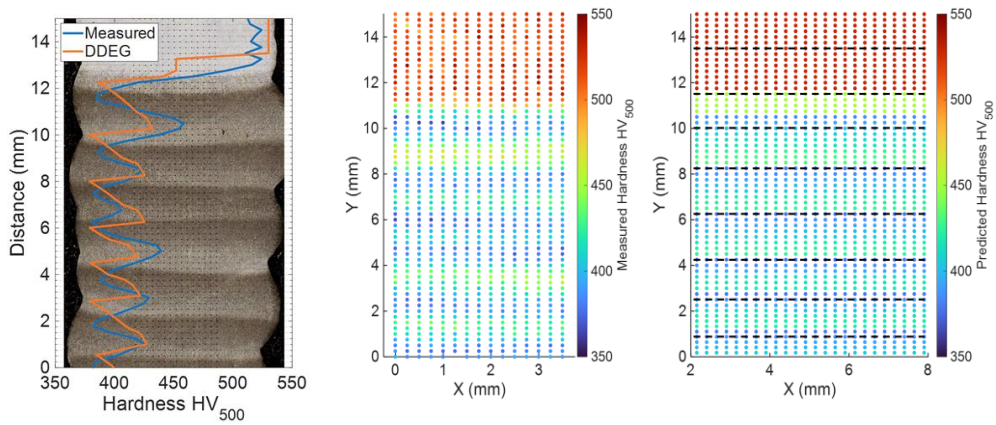

(a) (b) (c)

Fig. 9 Comparison of the experimental hardness value and predicted by calibrated DDEG model in a GMAWp WA-DED build of HSS

The hardness map in Fig. 9a was generated using LECO LM 100AT hardness mapper with 500g load and 250 μm step. The predicted hardness map in Fig. 9b was developed by FEA modeling of a GMAWp WA-DED processes using the respective processes parameters in Table 1, the calibrated DDGE heat source in Table 2, and a modified Grange-Baughman parameter (GBP) representing the tempering response in the tested HHS steel [42]. The GBP was previously modified to account for the effect of multiple reheat weld thermal histories on hardness reduction in weld metals and HAZs of low alloy steels [39,44,43,45,7,46,47].

The close correlation of predicted and experimentally measured hardness distribution shown in Fig. 8 and Fig. 9 demonstrates the benefit of using more expressive heat source models in FEA modeling of WAM processes. The performed validation study demonstrates that by calibrating the proposed DDEG and DEGC heat source models to precisely match the experimental fusion boundary lines, thermal histories and HAZ properties can be accurately predicted in FEA simulations. Comparison made between simulation using calibrated DDEG model and empirical DEG model provides evidence for effective improvement in simulation accuracy using our method. Comparison made between simulation using calibrated DDEG model and empirical DEG model, as shown in Fig. 7b, provides evidence for effective improvement in simulation accuracy using our method.

CONCLUSION

In this paper, we extended the existing double-ellipsoidal Gaussian (DEG) heat source model to more expressive DDEG and DEGC models that more accurately represent the heat transfer in the molten pool of GMAW and WA-DED processes. We also introduced a novel machine learning-accelerated framework for efficient heat source calibration. The calibrated DDEG and DEGC heat source models were validated and demonstrated by comparing FEA predicted and experimentally measured thermal histories and the hardness distributions in heat affected zones of welded and additively manufactured components.

References

[1] D. R. ATTHEY: 'A mathematical model for fluid flow in a weld pool at high currents', *Journal of Fluid Mechanics*, Vol. *98*, pp. 787-801, 1980.

[2] A. MAHRLE, J. SCHMIDT and D. WEISS: 'Simulation of temperature fields in arc and beam welding', *Heat and Mass Transfer*, Vol. *36*, pp. 117-126, 2000.

[3] K. C. MILLS, B. J. KEENE, R. F. BROOKS and A. SHIRALI: 'Marangoni effects in welding', *Philosophical Transactions of the Royal Society of London. Series A: Mathematical, Physical and Engineering Sciences*, Vol. *356*, pp. 911-925, 1998.

[4] G. M. OREPER and J. SZEKELY: 'Heat- and fluid-flow phenomena in weld pools', *Journal of Fluid Mechanics*, Vol. *147*, pp. 53, 1984.

[5] T. ZACHARIA, J. M. VITEK, J. A. GOLDAK, T. A. DEBROY, M. RAPPAZ and H. K. D. H. BHADESHIA: 'Modeling of fundamental phenomena in welds', *Modelling and Simulation in Materials Science and Engineering*, Vol. *3*, pp. 265-288, 1995.

[6] T. ZACHARIA, A. H. ERASLAN, D. K. AIDUN and S. A. DAVID: 'Three-dimensional transient model for arc welding process', *Metallurgical transactions. A, Physical metallurgy and materials science*, Vol. *20*, pp. 645-659, 1989.
[7] Y. LUO: *Process Optimization Framework for Temper Bead Welding Procedures*, Master Thesis, The Ohio State University, 2023.
[8] Y. LUO, E. JANG and B. ALEXANDROV: 'Computational Design of Experiment for Temper Bead Welding Design Optimization applied in Overlaying Nickel-based 625 Alloy on Grade 22 Steel', *In Submission*, 2025.
[9] R. I. KARLSSON and B. L. JOSEFSON: 'Three-Dimensional Finite Element Analysis of Temperatures and Stresses in a Single-Pass Butt-Welded Pipe', *Journal of Pressure Vessel Technology-transactions of The Asme*, Vol. *112*, pp. 76-84, 1990.
[10] J. GOLDAK, A. CHAKRAVARTI and M. BIBBY: 'A New Finite Element Model for Welding Heat Sources', *Metallurgical Transactions B*, Vol. *15*, pp. 299-305, 1984.
[11] D. ROSENTHAL: 'Mathematical Theory of Heat Distribution during Welding and Cutting', *Welding Journal*, Vol. *20*, pp. 220-234, 1941.
[12] E. FRIEDMAN: 'Thermomechanical Analysis of the Welding Process Using the Finite Element Method', *Journal of Pressure Vessel Technology-transactions of The Asme*, Vol. *97*, pp. 206-213, 1975.
[13] L.-E. LINDGREN: 'Finite Element Modeling and Simulation of Welding Part 1: Increased Complexity', *Journal of Thermal Stresses*, Vol. *24*, pp. 141-192, 2001.
[14] L.-E. LINDGREN: 'Finite Element Modeling and Simulation of Welding. Part 2: Improved Material Modeling', *Journal of Thermal Stresses*, Vol. *24*, pp. 195-231, 2001.
[15] L.-E. LINDGREN: 'Numerical modelling of welding', *Computer Methods in Applied Mechanics and Engineering*, Vol. *195*, pp. 6710-6736, 2006.
[16] M. A. WAHAB, M. J. PAINTER and M. H. DAVIES: 'The prediction of the temperature distribution and weld pool geometry in the gas metal arc welding process', *Journal of Materials Processing Technology*, Vol. *77*, pp. 233-239, 1998.
[17] P. R. DE FREITAS TEIXEIRA, D. B. DE ARAÚJO and L. A. B. DA CUNDA: 'Study of the gaussian distribution heat source model applied to numerical thermal simulations of TIG welding processes', *Science and Engineering Journal*, Vol. *23*, pp. 115-122, 2014.
[18] A. UR REHMAN, F. PITIR and M. SALAMCI: 'Full-Field Mapping and Flow Quantification of Melt Pool Dynamics in Laser Powder Bed Fusion of SS316L', *Materials*, Vol. *14*, pp. 6264, 2021.
[19] T. W. EAGAR and N. S. TSAI: 'Temperature fields produced by traveling distributed heat sources', Vol. *62*, pp. 346-355, 1983.
[20] J. GOLDAK, M. BIBBY, J. MOORE, R. HOUSE and B. PATEL: 'Computer modeling of heat flow in welds', *Metallurgical Transactions B*, Vol. *17*, pp. 587-600, 1986.
[21] A. ANCA, A. CARDONA, J. RISSO and V. D. FACHINOTTI: 'Finite element modeling of welding processes', *Applied Mathematical Modelling*, Vol. *35*, pp. 688-707, 2011.
[22] S. BARUAH and I. V. SINGH: 'A framework based on nonlinear FE simulations and artificial neural networks for estimating the thermal profile in arc welding', *Finite Elements in Analysis and Design*, Vol. *226*, pp. 104024, 2023.
[23] D. DENG and H. MURAKAWA: 'Numerical simulation of temperature field and residual stress in multi-pass welds in stainless steel pipe and comparison with experimental measurements', *Computational Materials Science*, Vol. *37*, pp. 269-277, 2006.
[24] D. GERY, H. LONG and P. G. MAROPOULOS: 'Effects of welding speed, energy input and heat source distribution on temperature variations in butt joint welding', *Journal of Materials Processing Technology*, Vol. *167*, pp. 393-401, 2005.

[25] J. GOLDAK, M. J. BIBBY, D. DOWNEY and M. GU: 'Heat and Fluid Flow in Welds', *Advanced Joining Technologies*, Springer Netherlands, pp. 69-82, https://doi.org/10.1007/978-94-009-0433-0_6, 1990.

[26] N. T. NGUYEN and J. H. CHUJUTALLI: 'Simulating Convective-Radiative Heat Sinks Effect by means of FEA-based Gaussian Heat Sources and Its Approximate Analytical Solutions for Semi-Infinite Body', https://doi.org/10.21203/rs.3.rs-458143/v1, 2021.

[27] A. K. UNNI and M. VASUDEVAN: 'Determination of heat source model for simulating full penetration laser welding of 316 LN stainless steel by computational fluid dynamics', *Materials Today: Proceedings*, Vol. *45*, pp. 4465-4471, 2021.

[28] J. H. CHUJUTALLI, M. I. LOURENÇO and S. F. ESTEFEN: 'Experimental-based methodology for the double ellipsoidal heat source parameters in welding simulations', *Marine Systems & Ocean Technology*, Vol. *15*, pp. 110-123, 2020.

[29] B. JOSHI, M.-R. AMINI, I. PARTALAS, F. IUTZELER and Y. MAXIMOV: 'Aggressive sampling for multi-class to binary reduction with applications to text classification', *Advances in neural information processing systems*, 2017.

[30] J. A. RAMOS-GREZ and M. SEN: 'Analytical, quasi-stationary Wilson-Rosenthal solution for moving heat sources', *International Journal of Thermal Sciences*, Vol. *140*, pp. 455-465, 2019.

[31] S. K. BATE, R. CHARLES and A. WARREN: 'Finite element analysis of a single bead-on-plate specimen using SYSWELD', *International Journal of Pressure Vessels and Piping*, Vol. *86*, pp. 73-78, 2009.

[32] Y. WANG, L. WANG, X. DI, Y. SHI, X. BAO and X. GAO: 'Simulation and analysis of temperature field for in-service multi-pass welding of a sleeve fillet weld', *Computational Materials Science*, Vol. *68*, pp. 198-205, 2013.

[33] C. LI, Y. SHI, Y. GU, D. FAN and M. ZHU: 'Effects of different activating fluxes on the surface tension of molten metal in gas tungsten arc welding', *Journal of Manufacturing Processes*, Vol. *32*, pp. 395-402, 2018.

[34] M. SEEGER: 'Gaussian Process For Machine Learning', *International Journal of Neural Systems*, Vol. *14*, pp. 69-106, 2004.

[35] D. P. KINGMA and J. BA: *Adam: A Method for Stochastic Optimization*, 2017.

[36] A. KRIZHEVSKY, I. SUTSKEVER and G. E. HINTON: 'ImageNet classification with deep convolutional neural networks', *Advances in neural information processing systems*, Vol. 25, Curran Associates, Inc., 2012.

[37] O. CHAMPAGNE and X.-T. PHAM: 'Numerical simulation of moving heat source in arc welding using the Element-free Galerkin method with experimental validation and numerical study', *International Journal of Heat and Mass Transfer*, Vol. *154*, pp. 119633, 2020.

[38] M. T. FORQUER: *Simplified Computational Modeling Approach for Analysis and Optimization of Temperbead Welding Procedures*, Master Thesis, The Ohio State University, 2018.

[39] J. STEWART: *Temper Bead Welding for Dissimilar Metal Welds and Overlays*, Ph.D. Thesis, The Ohio State University, 2019.

[40] F. NOGUEIRA: *Bayesian Optimization: Open source constrained global optimization tool for Python*, https://github.com/bayesian-optimization/BayesianOptimization, 2014.

[41] S. MATAN and B. ALEXANDROV: 'Computational Framework for Microstructure and Hardness Prediction in Fe-10Ni Welds', *In Submission to Welding Journal*, 2025.

[42] N. M. VEGA MICHALAK, B. ALEXANDROV, L. MCNEIL, D. HARWIG and P. FLATER: 'Understanding and Predicting the In-situ Tempering Effect during Wire-Arc Directed Energy Deposition of a High Strength Steel', *In Submission*, 2025.

[43] J. STEWART, B. ALEXANDROV and B. T. ALEXANDROV: 'Quantification of the hardness response in the heat-affected zone of low alloy steels subjected to temper bead welding', *Journal of Manufacturing Processes*, Vol. *66*, pp. 325-340, 2021.

[44] E. JANG, J. STEWART, Y. LUO, S. QU, ET AL.: 'Tempering Efficiency Evaluation for Dissimilar Weld Overlays', *Volume 1: Codes and Standards*, American Society of Mechanical Engineers, 2020.

[45] E. JANG, Y. LUO, B. ALEXANDROV, S. L. MCCRACKEN, J. TATMAN and D. BARBORAK: 'Quantification of the Tempering Response for Temper Bead Welding of SA-508 Low Alloy Steel', *Volume 1: Codes and Standards*, American Society of Mechanical Engineers, 2022.

[46] E. JANG, B. ALEXANDROV, S. MCCRACKEN and D. BARBORAK: 'Tempering Procedure Effects on the Impact Toughness in Simulated Heat Affected Zone of Grade 22 Steel', *Journal of Pressure Vessel Technology*, Vol. *146*, pp. 041501, 2024.

[47] E. JANG: *Tempering Kinetics and Carbide Precipitation in Low Alloy Steel Heat Affected Zones in Temper Bead Welding*, Ph.D. Thesis, The Ohio State University, 2025.